On-demand single-electron source via single-cycle acoustic pulses

Shunsuke Ota,[1,2] Junliang Wang,[3] Hermann Edlbauer,[3] Yuma Okazaki,[2] Shuji Nakamura,[2] Takehiko Oe,[2] Arne Ludwig,[4] Andreas D. Wieck,[4] Hermann Sellier,[3] Christopher Bäuerle,[3] Nobu-Hisa Kaneko,[2] Tetsuo Kodera,[1] and Shintaro Takada[2,*;†]

[1] *Department of Electrical and Electronic Engineering, Tokyo Institute of Technology, Tokyo 152-8550, Japan*

[2] *National Institute of Advanced Industrial Science and Technology (AIST), National Metrology Institute of Japan (NMIJ), 1-1-1 Umezono, Tsukuba, Ibaraki 305-8563, Japan*

[3] *Université Grenoble Alpes, CNRS, Grenoble INP, Institut Néel, Grenoble 38000, France*

[4] *Lehrstuhl für Angewandte Festkörperphysik, Ruhr-Universität Bochum, Universitätsstraße 150, Bochum 44780, Germany*

(Received 21 July 2023; revised 22 October 2023; accepted 18 January 2024; published 16 February 2024)

Surface acoustic waves (SAWs) are a reliable solution to the transport of single electrons with precision in piezoelectric semiconductor devices. Recently, highly efficient single-electron transport with a strongly compressed single-cycle acoustic pulse has been demonstrated. This approach, however, requires surface gates constituting the quantum dots, their wiring, and multiple gate movements to load and unload the electrons, which is very time-consuming. Here, on the contrary, we employ such a single-cycle acoustic pulse in a much simpler way—without any quantum dot at the entrance or exit of a transport channel—to perform single-electron transport between distant electron reservoirs. We observe the transport of a solitary electron in a single-cycle acoustic pulse via the appearance of the quantized acoustoelectric current. The simplicity of our approach allows for on-demand electron emission with arbitrary delays on a nanosecond time scale. We anticipate that enhanced synthesis of the SAWs will facilitate electron quantum optics experiments with multiple-electron flying qubits.

DOI: 10.1103/PhysRevApplied.21.024034

I. INTRODUCTION

Surface acoustic waves (SAWs) are mechanical waves that propagate along a material surface and accompany electric field modulation in piezoelectric materials. This property allows for exquisite spatial and temporal control of the local environment of electrons in solid systems. This control makes SAWs an interesting and promising method for electron transport in electron-quantum optics [1–9]. Recently, research has been conducted toward the realization of electron flying qubits as quantum information-processing devices [10].

In electron-quantum optics, single electrons are controlled using basic tools such as a single-electron source and a single-electron detector. These tools have been realized in several different systems [11–14], including the SAW system. In the SAW system, by combining these tools, single-electron transport over micrometers has been demonstrated [1,2,5] and coherent transport of electron spin has also been demonstrated [4,7].

A typical setup for a single-electron source using SAWs combines a quantum dot (QD), a transport channel, and an interdigital transducer (IDT). A single electron is prepared in the QDs and transported along the depleted transport channel by the SAWs. By using sufficiently strong SAWs, the transport of the electrons becomes highly robust and an electron is transferred while confined to a specific potential minimum of the SAWs [15]. This allows us to control the transfer timing of an electron and hence synchronized transfer of single electrons from multiple single-electron sources is possible. Recently, an electron-collision experiment using two synchronized single-electron sources in the SAW system has been demonstrated [9]. Another important development is a technique to generate a single-cycle SAW pulse using a chirped-interdigital transducer (a chirp-IDT) [16]. Employing the SAW pulse for single-electron transfer allows us to synchronize the timing of electron transport from multiple single-electron sources without picosecond-triggering each QD [5]. This is advantageous for scaling up the system, since we do not need to implement an rf line for each QD used as a single-electron source. On the other hand, in these previous studies, the single electron ejected has had to be prepared in the quantum dot first. Thus, each single-electron source has

*Corresponding author. takada@phys.sci.osaka-u.ac.jp

†Present address: Department of Physics, Graduate School of Science, Osaka University, Toyonaka, Osaka 560-0043, Japan

required a QD and a complex fast voltage sequence. This indicates that there is still room for improvement in the scalability of the system. Furthermore, the time-consuming electron preparation process is a speed-limiting factor for the entire electron flying qubit system that utilizes single electron charges in flight.

For metrology applications, regular SAWs are used with a depleted quantum rail consisting of two metal gates to realize a quantized current source [17–22]. Electric potential modulations accompanied by the SAWs pick up an integer number of electrons directly from the Fermi sea and transfer them over the quantum rail. As a result, the current, $I = nef$, where n is an integer, e is the elementary charge, and f is the frequency of the SAWs, has been observed. Here, when a single-cycle SAW pulse rather than regular SAWs is used with a depleted quantum rail, an on-demand single-electron source rather than a continuous quantized current source can be realized. In contrast to the single-electron source with a QD, the electron-capturing process before applying SAWs is not required. Hence, its operation could be faster. Furthermore, a chirp IDT can generate multiple SAW pulses with arbitrary delays, making it possible to generate single electrons with flexible arbitrary delays. So far, for metrology, high-accuracy electron pumping (an error rate $\leq 10^{-6}$) is reported in other methods [23–26]. SAW pumps have not been actively studied for standard application due to their limited accuracy (an error rate $\geq 10^{-4}$); nevertheless, their application to quantum information processing may not require the same level of high accuracy as the current standard and, as mentioned above, active research is under way.

Based on this idea, in this paper, we actualize an on-demand single-electron source consisting of a chirp IDT and a quantum rail for enabling the implementation of electron flying qubits with beam splitters [8,9]. We evaluate the performance of this single-electron source by repeatedly operating the single-electron source and by measuring the accuracy of the generated quantized current. In addition, we demonstrate that the delay between the successively transferred single electrons can be arbitrarily adjusted. Finally, we investigate the effect of electromagnetic crosstalk generated by driving the IDT on the accuracy of the single-electron source.

II. EXPERIMENTAL SETUP

The experiment is performed within a 4-K pulse-tube refrigerator. An Si-modulation-doped GaAs-AlGaAs heterostructure is used to fabricate the sample. The two-dimensional electron gas (2DEG) that is located at 110 nm below the surface has an electron density of $n \approx 2.8 \times 10^{11}$ cm^{-2} and a mobility of $\mu \approx 9 \times 10^5$ cm^2 V^{-1} s^{-1}. Figure 1(a) shows a schematic diagram of the device and the experimental setup. The device contains a quantum rail with a lithographic width of 0.8 μm and a length of 2 μm, defined by surface Schottky gates. The gates are made of a thin metal film consisting of 3-nm titanium and 14-nm gold. During the cool down of the device, a voltage of 0.35 V is applied to all the gates. The 2DEG around the gates is depleted by applying negative voltages. Figure 1(b) shows the conductance across the quantum rail as a function of the voltage V_t and V_b. For this measurement, we inject a current by applying a dc bias voltage (336 μV) to the contact O_r and measure the current recovered from the contact O_l. In the following measurements, we set the voltages V_t and V_b to be more negative than −2.1 V, where the current driven by the bias voltage does not flow. A chirp-IDT is placed on the sample surface 1.4 mm to the left of the quantum rail. The surface electrodes of the IDTs are made of a thin metal film consisting of 3-nm titanium and 27-nm aluminum. To reduce internal reflections at resonance, we employ a double-electrode pattern for the IDT. The IDT aperture is 30 μm and the SAW propagation direction is along [110]. The IDTs are designed and simulated with the homemade open-source PYTHON library IDTPY [27]. A signal for generating a SAW is produced by an arbitrary wave-form generator (AWG, Keysight M8190A). This signal subsequently passes through two high-frequency amplifiers (SHF S126A and Mini Circuits ZHL-4W-422+) at room temperature before being input into the chirp IDT. The generated SAW can be observed by a high-speed sampling oscilloscope (Keysight N1094B DCA-M) via the broadband detector IDT after being amplified by a broadband amplifier (SHF S126A) at room temperature.

III. SAW PULSE GENERATION

A chirp IDT [16] has a cell periodicity that changes gradually as shown in Fig. 1(a). Here, it is designed to generate SAWs with frequencies ranging from 0.5 to 3.0 GHz. By applying an appropriately time-dependent high-frequency voltage to this IDT, it is possible to generate strongly compressed SAW pulses. The gray solid line in Fig. 1(c) is a strongly compressed SAW pulse observed by the detector IDT. This wave form is distorted from the actual shape of the SAW that passes through the quantum rail, due to the frequency bandwidth of the detector. To find the wave form of the SAW transporting electrons, we performed a simulation using the impulse-response model. First, we simulated the wave form of the SAW including the detector-IDT component [light gray dotted line in Fig. 1(c)]. Then, by subtracting the detector-IDT component, the wave form of the SAW in the device was simulated [red dashed line in Fig. 1(c)]. The result indicates that a SAW pulse with one dominant minimum can be generated. What we would like to focus on here is the shape of the SAW pulse. This shape is optimized to smoothly pick up single electrons from the Fermi sea and transport them across the depleted quantum rail, and hence it differs from the shape used for the purpose of single electron transport using the

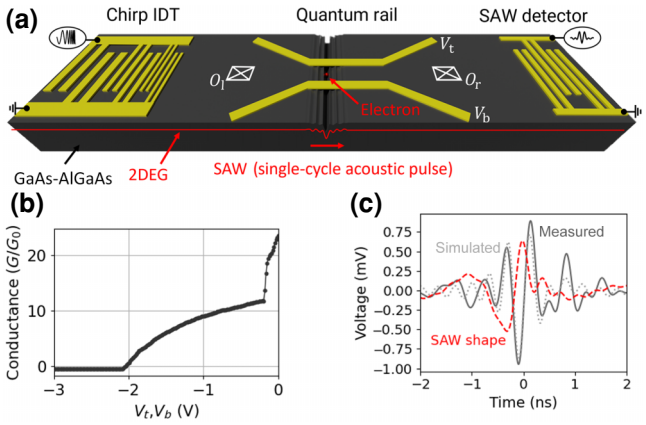

FIG. 1. (a) The experimental setup. A schematic of a chirp IDT emitting a compressed SAW toward a quantum rail and a broadband SAW detector, showing a perspective view of the sample that is realized via a metal surface gate in a GaAs-AlGaAs heterostructure. (b) The conductance across the quantum rail as a function of the voltages V_t and V_b. The current is measured from the ohmic contact O_l while applying a dc bias voltage (336 μV) to the ohmic contact O_r. $G_0 = 2e^2/h$, where e is the electron charge and h is the Planck constant. (c) The trace of the response of the broadband detector to the compressed SAW generated by the chirp IDT (gray solid line) with impulse-response simulation (light gray dotted line) and the corresponding SAW shape (red dashed line), which is derived by deconvolving the detector response to remove the contribution of the detector IDT in the simulation. The measurement is performed at 4 K.

QD. As a result of optimization, an asymmetric SAW pulse with a sharp edge after the minimum value was obtained.

IV. ON-DEMAND SINGLE ELECTRON SOURCE WITH SAW PULSES

It has been demonstrated that acoustoelectric currents can be generated by applying SAWs to a depleted quantum rail [17]. Here, the superposition of the longitudinal dynamic potential of the SAW and the transversal confinement potential of the quantum rail forms a train of moving QDs that picks up electrons from the Fermi sea and carries them across. The average number of electrons carried in each dynamic QD is determined at the entrance to the quantum rail by the balance between the potential gradient toward the entrance of the quantum rail and the confinement potential of the moving potential minima. When the potential gradient of the dynamic QD becomes steeper due to changes in the voltage of the quantum rail or the wave-form profile of the SAW, the spacing between the energy levels of the electrons in the QD widens and the charging energy of the QD increases. For a sufficiently large charging energy, the number of electrons within each dynamic QD is stably quantized. When each dynamic QD contains n electrons, where n is an integer number, the device works as a continuous quantized-electron source and generates a quantized current, $I = nef$, where f is the frequency of the sinusoidal SAW. Here, we investigate such a quantized current source with the single-cycle acoustic pulse shown above. By repeatedly sending the SAW pulse to the depleted quantum rail, we generate an observable quantized current and evaluate the accuracy of the single-electron transport by each SAW pulse from the stability of the current quantization. In this experiment, we set the repetition period of the SAW pulse to $T_{\rm cycle} =$ 1280 ns. When the number of electrons transported by each SAW pulse is quantized to an integer number n, the quantized current, $I = ne/T_{\rm cycle}$, is expected to be observed. Since we can arbitrarily control the timing of the SAW pulse generation with a chirp IDT, this electron source can be considered as an on-demand quantized electron source.

Figure 2 displays the acoustoelectric current as a function of the gate voltage of the quantum rail for different SAW amplitudes. When the gate voltage is swept to a more negative value, the potential gradient at the entrance of the quantum rail increases. As a result, a smaller number of electrons is transported across the depleted quantum rail by the SAW-dynamical potential. For the smaller SAW amplitude, the potential gradient of the SAW-dynamical potential is smaller and the charging energy of the dynamic QD at the entrance of the quantum rail is not large enough to have a stable number of electrons in each dynamic QD. This results in the acoustoelectric current smoothly decreasing as a function of the gate voltage. In contrast, for the larger SAW amplitude, the charging energy increases and a kink develops at $e/T_{\rm cycle}$. To evaluate the quantization of the acoustic electric current, we focus on the region where the gradient of the kink is the flattest, as indicated using red dots in Fig. 2. We have calculated the normalized difference,

$$I_{\rm N} = |(I_{\rm ave} - e/T_{\rm cycle})/(e/T_{\rm cycle})|,$$

between the average of measured acoustoelectric current $I_{\rm ave}$ and the ideal estimated value $e/T_{\rm cycle}$ with a combined standard uncertainty. The acoustic electric current took into account the current without SAW as offset and the gain of the current amplifier calibrated by a standard resistance. As a result of the calculation, in the flattest region (a gate-voltage width of 24 mV), the difference between the acoustoelectric current and the theoretical quantized current was 3.7% or less. (refer to Appendix A). This indicates that the kink caused by the SAW matched the ideal quantized current well. This result implies that in the kink, the average number of electrons in each SAW pulse is close to one. Around there, the device can be operated as an on-demand single electron source.

In this method, single electrons can be generated without preparing electrons, offering faster operation than conventional on-demand single-electron sources using SAWs. Additionally, the interval of the SAW pulses can be flexibly

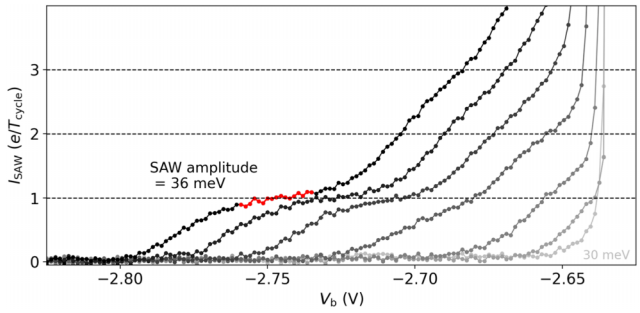

FIG. 2. The acoustoelectric current, I_{SAW}, induced by the compressed SAW pulse as a function of the voltage V_b with $V_t = -2.2$ V. The SAW amplitude varies from 30 meV to 36 meV (from right to left) (refer to Appendix B). The range indicated in red is a flat region where the gradient is less than a certain value of the leftmost curve (refer to Appendix A).

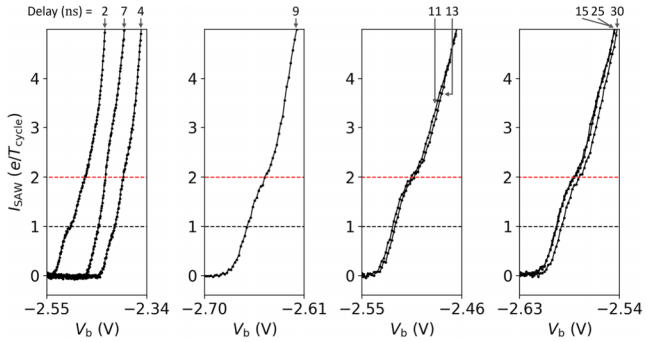

FIG. 3. The acoustoelectric current, I_{SAW}, as a function of the voltage V_b. Two SAW pulses within T_{cycle} with a changing delay between the pulses. The delay (in nanoseconds) is indicated above each curve. The red line indicates the expected quantized current $2e/T_{cycle}$. Each measurement was performed under optimal conditions (i.e., different gate voltages and cool downs) for the SAW pulse shape at each delay. Thus, the range of V_b was varied for each measurement. For clarity, each set of curves is displayed in a separate panel.

controlled, making it possible to generate single electrons with any desired delay, as discussed in Sec. V.

V. SINGLE-ELECTRON SOURCE WITH AN ARBITRARY DELAY

In Sec. IV, the interval between successive SAW pulses was set to 1280 ns, which is longer than the length of the SAW-generation signal of 130 ns. By setting the interval to be longer, the SAW-generation signals did not overlap each other. However, it is also possible to generate SAW pulses with shorter intervals by purposely overlapping the SAW-generation signals. In this section, we use this technique to verify the operation of a single-electron pump with arbitrarily controlled delay and explore its potential for high-speed operation. One limitation to keep in mind is the maximum output power of the high-frequency amplifier used: when two SAW-generation signals overlap, the maximum amplitude of the individual SAW pulses only reaches half the normal amplitude. This limitation reduces the flatness of the quantized current kink. Nevertheless, despite this reduced flatness, our data still exhibit distinguishable characteristics of a single-electron pump, in the form of the kinks seen in Fig. 3. Figure 3 presents the acoustoelectric current as a function of the gate voltages when we control the delay between two successive SAW pulses within T_{cycle} between 2 ns and 30 ns. The kinks will appear at $2e/T_{cycle}$ since we send two SAW pulses within T_{cycle}. For delays shorter than 9 ns, the kinks appear at unstable positions, whereas for delays larger than 9 ns, the $2e/T_{cycle}$ quantization current is stably observed. We attribute this result to the presence of small acoustic fluctuations before and after the main acoustic minimum. These extra fluctuations of the SAW pulse overlap with the main minimum of the other SAW pulse, preventing stable electron generation. When a chirp IDT with a wider-frequency bandwidth is developed, such extra fluctuation can be suppressed and a shorter delay time than 9 ns would be possible. In principle, the delay time can be shortened down to the width of the primary minimum, which is approximately 1 ns in this study. In our current chirp IDT, the delay can be arbitrarily controlled above 9 ns.

VI. EFFECT OF ELECTROMAGNETIC CROSSTALK

For stable electron-pump operation, the influence of electromagnetic crosstalk has to be taken into account. In the process of exciting an IDT to generate a SAW, an electromagnetic wave is concurrently emitted from the IDT. This emanation disrupts the surrounding potential of the nanostructures such as the quantum rail, thereby impeding the stability of the electron-pump operations. In previous single-electron transfer experiments with SAWs, the difference in velocity between SAWs ($v_{SAW} = 2.81$ μm/ns [15]) and electromagnetic waves has been used to avoid the simultaneous arrival of SAWs and electromagnetic waves at the nanostructures and to suppress the influence of such crosstalk. The influence of electromagnetic crosstalk on a single-electron pump using a standard IDT has been discussed and pointed out as an important problem previously [22]. There, the crosstalk was suppressed by the pulsed operation of the IDT and by avoiding the simultaneous arrival of SAWs and electromagnetic waves. When a standard IDT with a single resonant frequency is excited by pulsed sinusoidal waves, a narrow-frequency bandwidth of the standard IDT results in a finite rise (fall) time of SAWs, where a gradual change of the SAW amplitude makes single-electron pump operation unstable. As a result, it is not possible to avoid the influence of electromagnetic crosstalk with a standard IDT while maintaining highly accurate single-electron pump operation.

On the other hand, the SAW pulses generated by our chirp IDT have no rise (fall) time and only a single potential minimum that transports electrons. Therefore, we can arbitrarily switch the driving of the chirp IDT on and off without degrading the stability of the electron-pump operations. In the present device, from the distance between the IDT and the quantum rail, the SAW reaches the quantum rail approximately 505 ns after its generation at the IDT. The electromagnetic crosstalk propagates at the velocity of light and reaches the quantum rail immediately after its generation at the IDT. The influence of the crosstalk can be suppressed by shifting the timing of the SAW pulse arrival at the quantum rail and the timing of the SAW-generation signal input to the IDT, as shown in Fig. 4(a). Figure 4(b) shows the influence of the electromagnetic crosstalk on the acoustoelectric transport. Here, the number of SAW pulses within one cycle T_{cycle} is fixed at 2, only changing the timing of the SAW pulses. As a result, for one condition [the red curve in Fig. 4(b)], the SAW pulses and electromagnetic waves reach the quantum rail at the same time and hence the crosstalk effect exists. For the other case [the blue curve in Fig. 4(b)], by avoiding simultaneous arrival, the crosstalk effect is suppressed. When the crosstalk effect exists, stable electron pumping is disturbed and the acoustoelectric current changes smoothly as a function of the gate voltages. On the other hand, when the crosstalk effect is properly suppressed, a kink appears at the expected value of $2e/T_{\mathrm{cycle}}$.

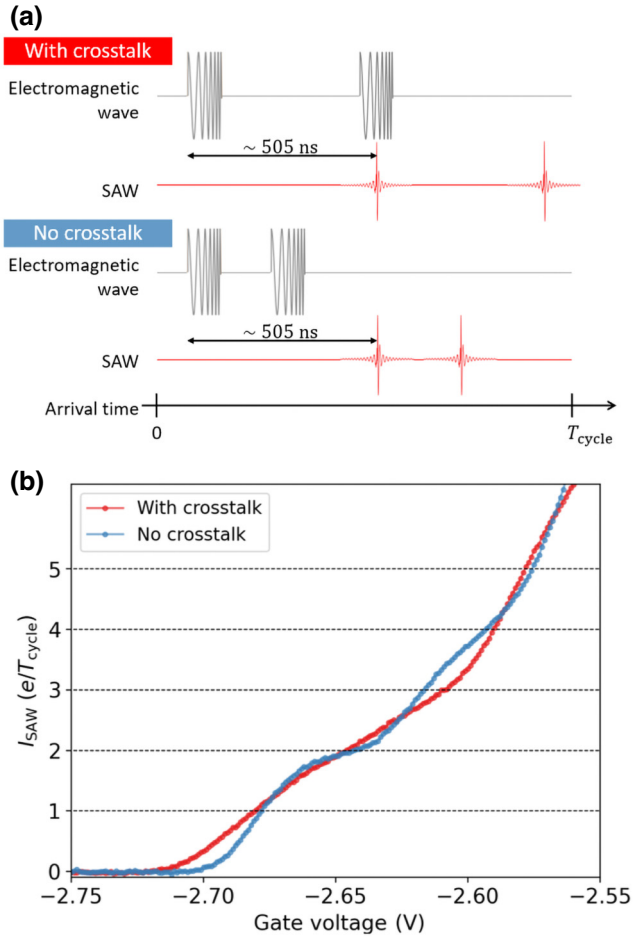

FIG. 4. (a) A schematic of the arrival time of electromagnetic waves and SAW pulses at the quantum rail. The SAW arrives at the quantum rail approximately 505 ns after generation at the IDT. (b) The acoustoelectric current, I_{SAW}, as a function of the voltage V_{b}, with $V_{\mathrm{t}} = -2.06$ V with and without crosstalk.

VII. SUMMARY AND OUTLOOK

In essence, we have demonstrated a simple on-demand single-electron source amalgamating chirp SAW pulses with a quantum rail. We have evaluated its performance from the observation of the quantized acoustoelectric current generated by repeatedly operating the source. Under the optimal operation conditions, there was a mismatch of 3.7% or less compared to the ideal operation. This single-electron source negates the need for dynamic gate operations to prepare a single electron into the QD, which stands in stark contrast to the previously demonstrated single-electron source with chirp SAW pulses [16]. Furthermore, we have demonstrated the flexible control of a delay between successive single-electron transfers. Meanwhile, the shortest delay time has been limited to 9 ns and the operation accuracy has been limited by the maximum available SAW amplitude. The former limitation could potentially be overcome by expanding the bandwidth of the chirp IDT. The latter could be ameliorated by enhancing the conversion efficiency between the IDT input signals and SAWs, which is achievable through the utilization of a thin film of stronger piezoelectric materials than GaAs, such as ZnO or AlN, or by fine tuning the impedance mismatch in the IDT. With these improvements, the accuracy of the single-electron pump operation will also be enhanced. As the width of the quantum rail (0.8 μm in this work) is much narrower than the wave front of the SAW (approximately 30 μm in this work and it can be even wider), synchronized operations of multiple single-electron sources can be implemented by simply putting multiple quantum rails within the wave front of a SAW. Notably, each quantum rail can be implemented with at least two or fewer static voltage inputs and does not require complex voltage manipulation. These characteristics facilitate the integration of many parallel single-electron sources and encourage scale-up of electron flying qubit architectures.

Another insight gained from this work is the impact of the potential shape of the SAW on electron transport. A SAW pulse, generated by a chirp IDT, is a superposition of broadband SAWs, thus permitting the deformation of the SAW pulse shape through appropriate adjustment of the input signal to the IDT. This study has required significant

deformation of the SAW pulse into an optimized asymmetric shape, in order to directly extract an electron from the Fermi sea instead of the QD. This indicates that the previously used symmetric SAW wave form was not the most suitable for electron transport and suggests the direction for further optimization. This insight is not only beneficial for research using SAW but also has implications for studies on the electron transport process in nanostructures [28,29].

Additionally, we have explored the effect of the electromagnetic field emitted directly from the IDT on the accuracy of the single-electron source. It has been presented as a factor in the degradation of the accuracy of electron transfer and pulse modulation of SAWs has been proposed as a solution in that context [22]. However, the narrow bandwidth of the IDT prevented fast enough pulse modulation to eliminate the influence of the electromagnetic crosstalk. In contrast, the large bandwidth of our chirp IDT and a single-cycle SAW pulse originating from it have allowed us to completely separate the timing of single-electron transfer across the quantum rail and the arrival of the electromagnetic crosstalk. We have clearly demonstrates that the elimination of the crosstalk indeed improves the accuracy of electron transport.

The results obtained in this study provide insights into single-electron transport with moving electric potentials and contribute to the field of single-electron quantum optics using SAWs, such as building up a flying qubit system or quantum communication with single-electron (or -hole) to single-photon conversion [30]. This study represents steady progress toward the realization of quantum systems using single electrons, hopefully providing techniques and insights that enrich the fundamental understanding of the field.

ACKNOWLEDGMENTS

S.O. acknowledges financial support from the Japan Science and Technology Agency (JST) "Support for Pioneering Research Initiated by the Next Generation Home" (SPRING) program, under Grant No. JPMJSP2106. J.W. acknowledges the European Union (EU) Horizon 2020 research and innovation program under the Marie Skłodowska-Curie Grant Agreement No. 754303. T.K. and S.T. acknowledge financial support from the Japan Society for the Promotion of Science (JSPS) KAKENHI Grant No. 20H02559. N.-H.K. acknowledges financial support from JSPS KAKENHI Grant No. JP18H05258. C.B. acknowledges financial support from the French Agence Nationale de la Recherche (ANR), project QUABS ANR-21-CE47-0013-01, as well as funding from the EU Horizon 2020 research and innovation program under Grant Agreement No. 862683, "UltraFastNano."

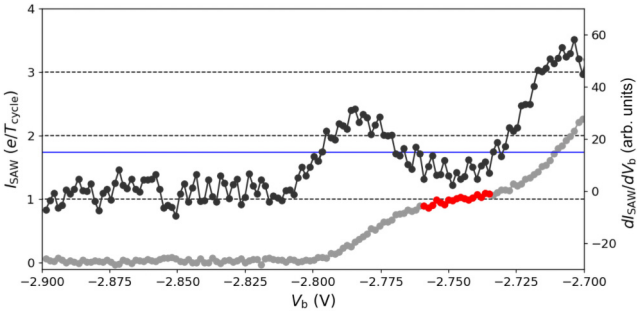

FIG. 5. The acoustoelectric current, I_{SAW}, of the maximum SAW amplitudes in Fig. 2 and its gradient. The left y axis represents I_{SAW} (gray and red), while the right y axis represents the gradient of I_{SAW} (black). The gradient is smoothed by averaging the values of the five neighboring points.

APPENDIX A: UNCERTAINTY OF THE ACOUSTOELECTRIC CURRENT

The normalized difference,

$$I_N = |(I_{ave} - e/T_{cycle})/(e/T_{cycle})|,$$

was calculated to be (0.037 ± 0.013) from the average of the measured acoustoelectric current I_{ave} and the ideal estimated value e/T_{cycle}. The average of the current value I_{ave} and the combined standard uncertainty were derived as follows: I_{ave} is the average of the measured values within the range in which the gradient becomes small and maintains a certain level of constancy. The range of a gradient smaller than -15 (the blue solid line in Fig. 5) was selected for our analysis as indicated in the red region in Fig. 5. As an offset, the average of the measured values where the zero current flow is subtracted and the uncertainty of the transimpedance amplifier (DDPCA-300) are also factored in. The gain of the transimpedance amplifier was calibrated using high-ohm standard resistors calibrated by national resistance standards. We utilized a combined standard uncertainty that included the gain uncertainty of the transimpedance amplifier and the standard uncertainty derived from the current measurements.

APPENDIX B: SAW-AMPLITUDE ESTIMATION

The amplitude of the SAW when using chirp pulses has been estimated in a previous report [16] by comparison with the SAW stemming from the normal IDT. This previous report and the experiment in this paper were performed with the same setup and the same substrate. From the power-to-energy conversions that have been obtained, the amplitude of the compressed SAW pulse generated by the input power to the chirp IDT of 28.6 dBm (30.1 dBm) sent from room temperature to the cryogenic setup is estimated to be 30 meV (36 meV) in the data of Fig. 2. We mainly used SAWs with an amplitude of 30 meV in other

measurements. In Fig. 3, each SAW pulse is half the amplitude as a result of overlapping input wave forms and hence 15 meV. Because the condition of the quantum rail changes due to the recooling of the sample, the gate-voltage condition at which the kink appears is different in the results of each figure, even though the SAW amplitude is the same for each measurement.

[1] S. Hermelin, S. Takada, M. Yamamoto, S. Tarucha, A. D. Wieck, L. Saminadayar, C. Bäuerle, and T. Meunier, Electrons surfing on a sound wave as a platform for quantum optics with flying electrons, Nature **477**, 435 (2011).

[2] R. P. G. McNeil, M. Kataoka, C. J. B. Ford, C. H. W. Barnes, D. Anderson, G. A. C. Jones, I. Farrer, and D. A. Ritchie, On-demand single-electron transfer between distant quantum dots, Nature **477**, 439 (2011).

[3] J. A. H. Stotz, R. Hey, P. V. Santos, and K. H. Ploog, Coherent spin transport through dynamic quantum dots, Nat. Mater. **4**, 585 (2005).

[4] B. Bertrand, S. Hermelin, S. Takada, M. Yamamoto, S. Tarucha, A. Ludwig, A. D. Wieck, C. Bäuerle, and T. Meunier, Fast spin information transfer between distant quantum dots using individual electrons, Nat. Nanotechnol. **11**, 672 (2016).

[5] S. Takada, H. Edlbauer, H. V. Lepage, J. Wang, P.-A. Mortemousque, G. Georgiou, C. H. W. Barnes, C. J. B. Ford, M. Yuan, P. V. Santos, X. Waintal, A. Ludwig, A. D. Wieck, M. Urdampilleta, T. Meunier, and C. Bäuerle, Sound-driven single-electron transfer in a circuit of coupled quantum rails, Nat. Commun. **10**, 4557 (2019).

[6] P. Delsing *et al.*, The 2019 surface acoustic waves roadmap, J. Phys. D: Appl. Phys. **52**, 353001 (2019).

[7] B. Jadot, P.-A. Mortemousque, E. Chanrion, V. Thiney, A. Ludwig, A. D. Wieck, M. Urdampilleta, C. Bäuerle, and T. Meunier, Distant spin entanglement via fast and coherent electron shuttling, Nat. Nanotechnol. **16**, 570 (2021).

[8] R. Ito, S. Takada, A. Ludwig, A. D. Wieck, S. Tarucha, and M. Yamamoto, Coherent beam splitting of flying electrons driven by a surface acoustic wave, Phys. Rev. Lett. **126**, 070501 (2021).

[9] J. Wang, H. Edlbauer, A. Richard, S. Ota, W. Park, J. Shim, A. Ludwig, A. D. Wieck, H.-S. Sim, M. Urdampilleta, T. Meunier, T. Kodera, N.-H. Kaneko, H. Sellier, X. Waintal, S. Takada, and C. Bäuerle, Coulomb-mediated antibunching of an electron pair surfing on sound, Nat. Nanotechnol. **18**, 721 (2023).

[10] H. Edlbauer *et al.*, Semiconductor-based electron flying qubits: Review on recent progress accelerated by numerical modelling, EPJ Quantum Technol. **9**, 21 (2022).

[11] G. Fève, A. Mahé, J.-M. Berroir, T. Kontos, B. Plaçais, D. C. Glattli, A. Cavanna, B. Etienne, and Y. Jin, An on-demand coherent single-electron source, Science **316**, 1169 (2007).

[12] J. Dubois, T. Jullien, F. Portier, P. Roche, A. Cavanna, Y. Jin, W. Wegscheider, P. Roulleau, and D. C. Glattli, Minimal-excitation states for electron quantum optics using levitons, Nature **502**, 659 (2013).

[13] T. Jullien, P. Roulleau, B. Roche, A. Cavanna, Y. Jin, and D. C. Glattli, Quantum tomography of an electron, Nature **514**, 603 (2014).

[14] R. Bisognin, A. Marguerite, B. Roussel, M. Kumar, C. Cabart, C. Chapdelaine, A. Mohammad-Djafari, J.-M. Berroir, E. Bocquillon, B. Plaçais, A. Cavanna, U. Gennser, Y. Jin, P. Degiovanni, and G. Fève, Quantum tomography of electrical currents, Nat. Commun. **10**, 3379 (2019).

[15] H. Edlbauer, J. Wang, S. Ota, A. Richard, B. Jadot, P.-A. Mortemousque, Y. Okazaki, S. Nakamura, T. Kodera, N.-H. Kaneko, A. Ludwig, A. D. Wieck, M. Urdampilleta, T. Meunier, C. Bäuerle, and S. Takada, In-flight distribution of an electron within a surface acoustic wave, Appl. Phys. Lett. **119**, 114004 (2021).

[16] J. Wang, S. Ota, H. Edlbauer, B. Jadot, P.-A. Mortemousque, A. Richard, Y. Okazaki, S. Nakamura, A. Ludwig, A. D. Wieck, M. Urdampilleta, T. Meunier, T. Kodera, N.-H. Kaneko, S. Takada, and C. Bäuerle, Generation of a single-cycle acoustic pulse: A scalable solution for transport in single-electron circuits, Phys. Rev. X **12**, 031035 (2022).

[17] J. M. Shilton, D. R. Mace, V. I. Talyanskii, Y. Galperin, M. Y. Simmons, M. Pepper, and D. A. Ritchie, On the acoustoelectric current in a one-dimensional channel, J. Phys.: Condens. Matter **8**, L337 (1996).

[18] V. I. Talyanskii, J. M. Shilton, M. Pepper, C. G. Smith, C. J. B. Ford, E. H. Linfield, D. A. Ritchie, and G. A. C. Jones, Single-electron transport in a one-dimensional channel by high-frequency surface acoustic waves, Phys. Rev. B **56**, 15180 (1997).

[19] J. Cunningham, V. I. Talyanskii, J. M. Shilton, M. Pepper, M. Y. Simmons, and D. A. Ritchie, Single-electron acoustic charge transport by two counterpropagating surface acoustic wave beams, Phys. Rev. B **60**, 4850 (1999).

[20] J. Cunningham, V. I. Talyanskii, J. M. Shilton, M. Pepper, A. Kristensen, and P. E. Lindelof, Single-electron acoustic charge transport on shallow-etched channels in a perpendicular magnetic field, Phys. Rev. B **62**, 1564 (2000).

[21] J. Ebbecke, K. Pierz, and F. Ahlers, Influence of the shape of a quasi-one-dimensional channel on the quantized acousto-electric current, Phys. E (Amsterdam, Neth.) **12**, 466 (2002).

[22] M. Kataoka, C. J. B. Ford, C. H. W. Barnes, D. Anderson, G. A. C. Jones, H. E. Beere, D. A. Ritchie, and M. Pepper, The effect of pulse-modulated surface acoustic waves on acoustoelectric current quantization, J. Appl. Phys. **100**, 063710 (2006).

[23] M. D. Blumenthal, B. Kaestner, L. Li, S. Giblin, T. J. B. M. Janssen, M. Pepper, D. Anderson, G. Jones, and D. A. Ritchie, Gigahertz quantized charge pumping, Nat. Phys. **3**, 343 (2007).

[24] F. Stein, D. Drung, L. Fricke, H. Scherer, F. Hohls, C. Leicht, M. Götz, C. Krause, R. Behr, E. Pesel, K. Pierz, U. Siegner, F. J. Ahlers, and H. W. Schumacher, Validation of a quantized-current source with 0.2 ppm uncertainty, Appl. Phys. Lett. **107**, 103501 (2015).

[25] G. Yamahata, S. P. Giblin, M. Kataoka, T. Karasawa, and A. Fujiwara, Gigahertz single-electron pumping in silicon with an accuracy better than 9.2 parts in 107, Appl. Phys. Lett. **109**, 013101 (2016).

[26] M. W. Keller, J. M. Martinis, N. M. Zimmerman, and A. H. Steinbach, Accuracy of electron counting using a 7-junction electron pump, Appl. Phys. Lett. **69**, 1804 (1996).
[27] J. Wang, Junliang-wang/IDTPY: First release (2022).
[28] V. Langrock, J. A. Krzywda, N. Focke, I. Seidler, L. R. Schreiber, and Ł. Cywiński, Blueprint of a scalable spin qubit shuttle device for coherent mid-range qubit transfer in disordered Si/SiGe/SiO_2, PRX Quantum **4**, 020305 (2023).
[29] I. Seidler, T. Struck, R. Xue, N. Focke, S. Trellenkamp, H. Bluhm, and L. R. Schreiber, Conveyor-mode single-electron shuttling in Si/SiGe for a scalable quantum computing architecture, npj Quantum Inf. **8**, 100 (2022).
[30] T. K. Hsiao, A. Rubino, Y. Chung, S. K. Son, H. Hou, J. Pedrós, A. Nasir, G. Éthier-Majcher, M. J. Stanley, R. T. Phillips, T. A. Mitchell, J. P. Griffiths, I. Farrer, D. A. Ritchie, and C. J. B. Ford, Single-photon emission from single-electron transport in a SAW-driven lateral light-emitting diode, Nat. Commun. **11**, 917 (2020).